Available online at www.sciencedirect.com

ScienceDirect

J Materiomics 2 (2016) 179–186

www.ceramsoc.com/en/

www.journals.elsevier.com/journal-of-materiomics/

Enhanced thermoelectric performance of chalcogenide $Cu_2CdSnSe_4$ by ex-situ homogeneous nanoinclusions

Qiufan Chen [a], Yanci Yan [a], Heng Zhan [a], Wei Yao [a], Yan Chen [b], Jiyan Dai [b], Xiaonan Sun [a,*], Xiaoyuan Zhou [a,*]

[a] *Department of Applied Physics, Chongqing University, Chongqing 400044, China*

[b] *Department of Applied Physics, The Hong Kong Polytechnic University, Kowloon, Hong Kong, China*

Received 19 February 2016; accepted 4 May 2016

Available online 13 May 2016

Abstract

Quaternary chalcogenide $Cu_2CdSnSe_4$ distributed with ex-situ homogeneous nanoinclusions has been synthesized by ball milling, followed by spark plasma sintering. The $Cu_2CdSnSe_4$ nanocrystallites with sizes ranging from 20 to 30 nm were prepared via colloidal synthesis, while the $Cu_2CdSnSe_4$ matrix was made by the traditional solid state reaction method. It is found that nanocrystallite inclusions strongly enhance electrical conductivity while preserving the Seebeck coefficient. In addition, these inclusions significantly reduce the lattice thermal conductivity through scattering phonons with all-scale length due to the polymorphous structure feature of $Cu_2CdSnSe_4$ composites. These concomitant effects result in an enhanced thermoelectric performance with the dimensionless figure of merit ZT reaching a peak value of 0.5 at 760 K, which is a 65% improvement compared to that of the pure $Cu_2CdSnSe_4$ matrix. These observations demonstrate an exciting scientific opportunity to raise the figure of merit via ex-situ homogeneous nanoinclusions, not only for quaternary chalcogenides but also for other promising thermoelectric materials.

Keywords: Quaternary chalcogenide; Homogeneous inclusions; Phonon scattering; Thermoelectric performance

1. Introduction

The confluence of energy demands and environmental protection have spurred research into renewable technologies, which will have a revolution in energy consumption from traditional extensive modes (fossil fuels) to sustainable clean energy. Among these technologies, thermoelectric (TE) devices can convert heat energy to electricity directly. The efficiency of TE materials is determined by the dimensionless figure of merit $ZT = S^2\sigma T/\kappa$, where S, σ, and κ are the Seebeck coefficient, electrical conductivity, and thermal conductivity, respectively. Two main strategies for improving TE performance are enhancing electrical properties and reducing thermal conductivity. However, due to the inter-correlation between these TE parameters, simultaneous optimization for all these transport parameters becomes a subject of great importance in TE technology. For example, σ usually decreases with any attempt to increase S. Striking progress has been made in the search for higher performance TE materials [1–11].

Due to their intensive phonon scattering induced by intrinsic hierarchical chemical-bond strength and atomic level structural distortions, the class of quaternary chalcogenide compounds I_2-II-IV-VI_4 (I=Ag, Cu; II=Zn, Cd; IV=Si, Ge, Sn; VI=S, Se, Te) with diamond-like structures and wide band gaps possess low lattice thermal conductivities. As such, quaternary chalcogenides have been attracting worldwide

* Corresponding authors. Tel.: +86 023 6567 8551.

E-mail addresses: xnsun168@cqu.edu.cn (X. Sun), xiaoyuan2013@cqu.edu.cn (X. Zhou).

Peer review under responsibility of The Chinese Ceramic Society.

http://dx.doi.org/10.1016/j.jmat.2016.05.009

attention. Current strategies to improve *ZT* values of quaternary chalcogenides are focusing on maximizing the power factor through substitutional doping and further reducing the thermal conductivity via diverse preparation methods. So far, a *ZT* value of 0.91 at 700 K, which is the record *ZT* to date, has been achieved in Cu-rich $Cu_{2.1}Zn_{0.9}SnSe_4$ by the traditional solid-state reaction method [12]. Furthermore, this value is nearly comparable to that in classical *p*-type thermoelectric materials, such as fully filled skutterudites and commercial Bi_2Te_3-based materials. Meanwhile, colloidal synthesis has been widely used to successfully prepare chalcogenide nanocrystals, and peak *ZT* values of 0.65 at 723 K for $Cu_{2.1}Cd_{0.8}SnSe_{3.4}$ [13] and 0.8 at 688 K for $Cu_{1.7}Ag_{0.3}CdSnSe_4$ [14] have been reported.

Another promising approach to improve TE performance is to form bulk nanocomposites, in which different forms of nanoinclusions are distributed in the matrix. Examples are Ag [15], TiO_2 [16], C_{60} [17], ZrO_2 [18], and NiSb [19] embedded in skutterudite matrices; SiC nanodispersions in PbTe-based thermoelectric nanocomposites [20]; and hierarchical nanostructured β-Zn_4Sb_3–Cu_3SbSe_4 [21] or β-Zn_4Sb_3 alloy bulk embedded with$(Bi_2Te_3)_{0.2}(Sb_2Te_3)_{0.8}$ [22]. Provided that the phonon mean free path is reduced by enhanced phonon boundary scattering of a degree higher than any reduction in the mean free path of charge carriers, significantly reduced thermal conductivities can be obtained by this approach without a negative effect on electrical properties (with a positive effect in some cases), eventually leading to improvement of the figure of merit. Such nanostructured composites are fabricated using bulk processing routes via mechanical mixing or in-situ reaction methods rather than nanofabrication means. Therefore, the synthesis is scalable and compatible with industrial processing [16]. However, impurities, such as oxygen brought by ball milling, exert a negative impact on the electronic transport properties. While the contamination problem can be substantially avoided by using an *in-situ* reaction method, the control of composition, grain size and distribution of these *in-situ* nanoinclusions is, nonetheless, a great challenge. As a consequence, all these methods are limited by their "impurities" extraneous to the matrix. On the other hand, homogeneous nanoinclusions are another type of inclusion dispersed in the matrix via an ex-situ technique. Such inclusions have identical composition and structure to the matrix, and they may avoid the problems mentioned above.

In this paper, by analyzing quaternary chalcogenide nanocomposites ($Cu_2CdSnSe_4$), we demonstrate that by dispersing ex-situ homogeneous nanoinclusions, TE performance of chalcogenide nanocomposites can be greatly enhanced. $Cu_2CdSnSe_4$ nanocrystallites without the presence of any impurity phase were obtained via colloidal synthesis. Single phase $Cu_2CdSnSe_4$ matrix was fabricated by the traditional solid state reaction method. Subsequently, $Cu_2CdSnSe_4$ nanocomposites possessing the polymorphous structure feature were obtained by dispersing $Cu_2CdSnSe_4$ nanocrystallites (0–5 vol.%) into the matrix via a ball milling process. It is found that the electrical conductivity of $Cu_2CdSnSe_4$ nanocomposites is enhanced due to the increasing carrier concentration. Meanwhile, the reduction of the lattice thermal conductivity is achieved due to the enhanced scattering of phonons with mid- to long-wavelengths by the embedded nanoparticles, which was observed on the grain boundary and surface in $Cu_2CdSnSe_4$ nanocomposites [23]. A *ZT* up to 0.50 at 760 K is yielded when incorporating 1% nanocrystallites, which is roughly a 65% enhancement compared to that of the pure matrix.

2. Experimental

$Cu_2CdSnSe_4$ nanocrystallites were prepared using colloidal synthesis. In a typical fabrication, a precursor sol of $Cu_2CdSnSe_4$ was prepared by first dissolving copper acetylacetonate (3.9 mmol), cadmium acetate dehydrate (1.0 mmol), and acetylacetone tin(IV) dichloride salt (1.8 mmol) in 10 mL oleylamine under vacuum conditions; heating the mixture to 413 K; and then maintaining it at this temperature for 30 min. The temperature of this mixture was then dropped to 373 K and kept at this temperature until the selenium solution was injected. At the same time, 8 mmol selenium dioxide was dissolved in 1-octadecene under vacuum conditions at 353 K until the color of this solution became orange. This solution was then cooled to 330 K and rapidly injected into the former solution. The temperature of the mixture was increased to 553 K under nitrogen flow and maintained for 30 min. When the reaction finished, the solution was cooled naturally to 330 K. The brown-black product was collected and centrifuged at 8000 rpm for 5 min. The upper orange solution was discarded, and then hexane and ethanol were added to disperse the nanocrystals. The washing procedure was repeated at least five times until the prepared nanocrystal precipitate could not be dispersed in hexane. To completely remove the surfactant, the nanocrystals washed by hexane and ethanol were suspended in a mixture of hydrazine hydrate and hexane with a volume radio of 1:1 and stirred for approximately 12 h. This process was repeated three times. Finally, the washed samples were collected through centrifugation and dried out in a vacuum dryer.

$Cu_2CdSnSe_4$ matrices were synthesized by a solid-state reaction, followed by ball milling and spark plasma sintering. Pure elemental Cu (99.999%, rod), Cd (99.99%, granulous), Sn (99.999%, pellet), and Se (99.999%, pellet) were weighed according to the stoichiometric ratio and sealed in the evacuated quartz ampoules. The sealed ampoules were slowly heated to 973 K at a rate not exceeding 5 K/min, held at that temperature for 10 h, and then cooled to room temperature. The resultant alloys were ground in an agate mortar. After that, the powders were sealed and annealed at 973 K for 84 h. The final ingots were ground in the agate mortar, followed by a Fritsch planetary ball milling machine (Pulverisette 7) with agate balls at 200 rpm for 2 h. Afterwards, $Cu_2CdSnSe_4$ nanocrystallites with sizes from 20 to 30 nm were dispersed into the $Cu_2CdSnSe_4$ matrix at 200 rpm for 20 min using a ball milling process, which was carried out inside a glove box to prevent any contamination of oxygen. The final step was spark plasma sintering of this mixture with a graphite die ($\Phi = 10$ mm) at 753 K for 5 min under a pressure of 45 MPa.

High-temperature electrical conductivity (σ) and the Seebeck coefficient (S) were measured on rectangular-shaped samples at temperatures from 300 to 760 K using a commercial system (LSR-3, Linseis Messgeraete GmbH, Selb, Germany). Thermal diffusivity (λ) was obtained by the laser flash method (Netzsch LFA-457) and converted into thermal conductivity (κ) using $\kappa=\lambda C_p d$, where C_p is the specific heat measured in a differential scanning calorimeter (Netzsch, 404 F3). The room-temperature carrier concentration was measured via a homemade apparatus in an applied field of ±1 T, and the carrier mobility μ was calculated according to the equation $\sigma = nq\mu$. The sample density d was calculated with the Archimedes method, and the densities of the samples with 0%, 1%, 3% and 5% nanocrystallites were 5.6 g/cm^3, 5.7 g/cm^3, 5.8 g/cm^3 and 5.8 g/cm^3, respectively. Powder X-ray diffraction patterns were collected using a PANalytical X'pert apparatus with Cu Ka radiation. The experimental details of Raman were performed by a commercial Micro-Raman spectrometer (Horiba Jobin Yvon S.A.S) with a 532 nm laser and a 50 × objective. The morphology and microstructure were investigated using field emission scanning electron microscopy (JSM-7800F, JEOL) and transmission electron microscopy (JEM2100F).

3. Results and discussion

3.1. Structural characterization

As shown in Fig. 1(a), the $Cu_2CdSnSe_4$ nanocrystallites heat treated at 553 K for 30 min possess a pure zinc-blende structure without the presence of any impurity phases (documented by the peaks indexed to PDF#52-869). Fig. 1(b) and (c) show the typical scanning electron microscopy (SEM) and transmission electron microscopy (TEM) images of $Cu_2CdSnSe_4$ nanocrystallites. The as-prepared nanocrystallites are narrowly distributed, and the average size of the nanoparticles is about 25 nm. The excellent control of the particle size is achieved by the wet chemistry approach. In addition, the specific size of the as-prepared nanoparticles is dependent on both the species and the concentration of the precursor solutions as well as the temperature and volume of the reaction vessel. High-resolution transmission electron microscopy (HRTEM) and selected-area electron diffraction patterns are shown in Fig. 1(d), where one can see that the as-prepared nanocrystallites are mainly of zinc-blende structure.

Fig. 2(a) shows X-ray diffraction (XRD) patterns of the $Cu_2CdSnSe_4$ nanocomposites, which are indexable to the stannite-type $Cu_2CdSnSe_4$ with space group $I\bar{4}2m$ (PDF#52-869). It is noted that there is no new phase, and phase segregation occurs after spark plasma sintering (SPS). Such pure phases of $Cu_2CdSnSe_4$ nanocomposites were obtained by the relatively short ball milling time and rate, leading to minimized contamination and lattice strain build-up, which might otherwise have a detrimental effect on the electronic mobility [24–27]. Because the diffraction patterns of the Cu_xSe and Cu_2SnSe_3 phases are similar to or even overlapped with that of $Cu_2CdSnSe_4$ compounds, it is still difficult to confirm that a completely pure phase of $Cu_2CdSnSe_4$ is obtained by only judging from XRD patterns. As such, room-temperature Raman spectra were generated to further confirm the structure. The results are shown in Fig. 2(b). As we know, $Cu_2CdSnSe_4$ should exhibit the most intense peaks at

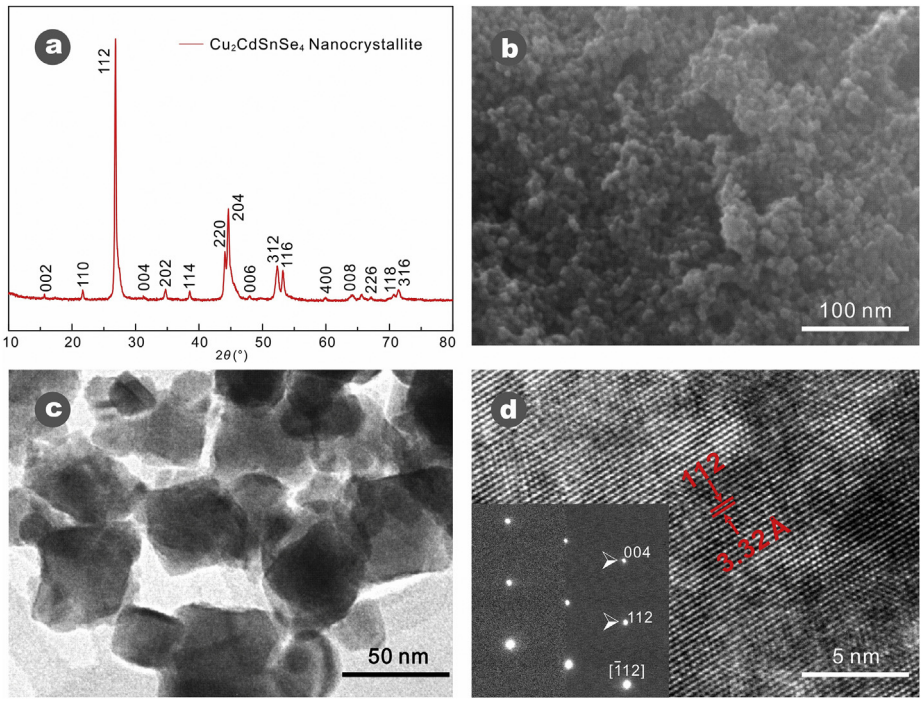

Fig. 1. (a) X-ray diffraction patterns; (b) typical SEM image; (c) low-magnification TEM image; and (d) HRTEM image of the as-prepared $Cu_2CdSnSe_4$ nanocrystallites and selected-area electron diffraction pattern (inset of d).

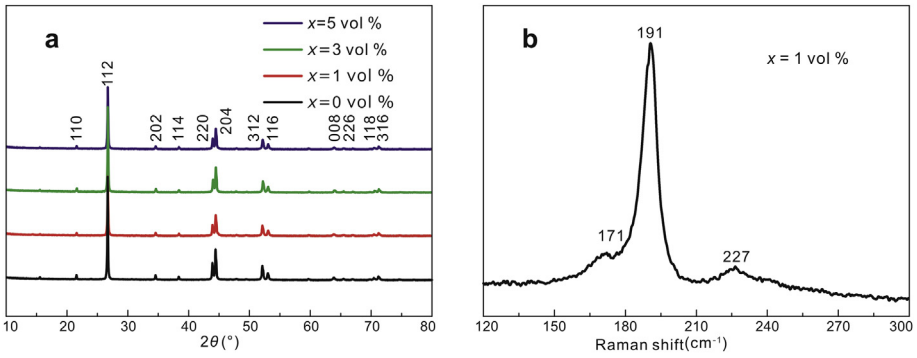

Fig. 2. (a) XRD patterns; (b) Raman spectra of the $Cu_2CdSnSe_4$ nanocomposite ($x = 1$ vol.%).

170–171 and 194–196 cm^{-1} and a less intense peak at 231 cm^{-1}, while Cu_2SnSe_3 and Cu_xSe phases show peaks at 180 and 260–265 cm^{-1}, respectively. As displayed in Fig. 2(b), three peaks located at 171, 191, and 227 cm^{-1} match perfectly with the tetragonal $Cu_2CdSnSe_4$ phase [28,29]. Some red shift can be observed because Raman spectroscopy is sensitive to the grain size and defects in the samples [30,31]. Combined with the XRD pattern, we believe that the $Cu_2CdSnSe_4$ bulk possesses a pure tetragonal phase rather than a mixture of binary or ternary compounds.

The fracture surface morphology of the $Cu_2CdSnSe_4$ matrix and the nanocomposite with x equaling 1 vol.% $Cu_2CdSnSe_4$ nanocrystallite are shown in Fig. 3(a) and (b), respectively. It is apparent that these samples possess sharp and clean grain boundaries, which are believed to be beneficial for the charge transport. In addition, some nanoparticles with sizes ranging from 20 to 30 nm were observed at grain boundaries and on the grain surface in $Cu_2CdSnSe_4$ nanocomposites. It is straightforward to consider them as the dispersed $Cu_2CdSnSe_4$ nanocrystallites because they are completely absent from the pure matrix. The exact composition of these nanoparticles is confirmed by energy-dispersive X-ray (EDX) spectra in TEM as described below. As reported in previous studies [32–37], such nanoparticles are considered to be effective in scattering

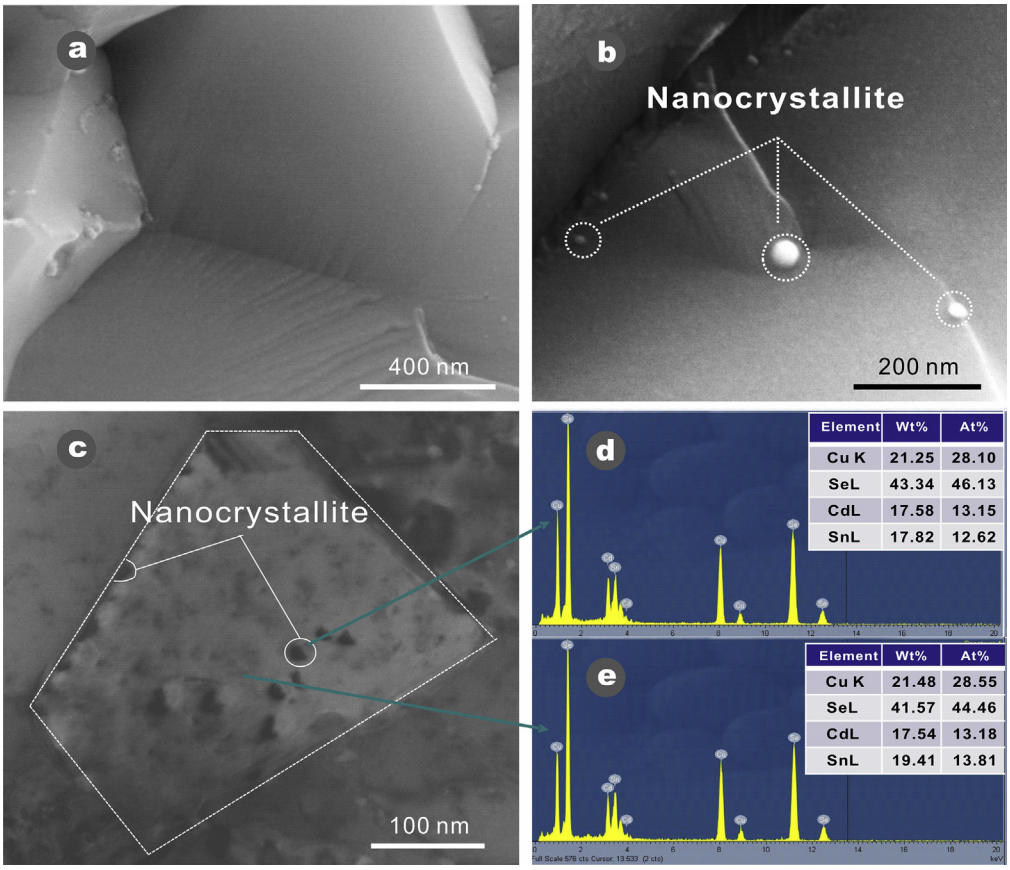

Fig. 3. Fracture surface morphology of $Cu_2CdSnSe_4$ matrix (a) and fracture surface of nanocomposite with $x = 1$ vol.% (b); (c) low-magnification TEM image of the nanocomposite with $x = 1$ vol.%; (d) and (e) are the EDX spectra of the nanocrystallites and the surrounding matrix, respectively.

phonons with both mid- and long-wavelengths, providing an additional mechanism to reduce the thermal conductivity. Fig. 3(c) displays the low magnification TEM image for the $Cu_2CdSnSe_4$ nanocomposite ($x = 1$ vol.%), which further confirms that the embedded nanoparticles with diameters of approximately 20 nm are on grain surfaces and boundaries. Moreover, results from the EDX spectra, shown in Fig. 3(d) and (e), strongly indicate the chemical composition of nanocrystallites at both the grain boundary and the surrounding matrix is $Cu_2CdSnSe_4$. Judging from SEM and TEM images, it is noted that the size and shape of these $Cu_2CdSnSe_4$ nanocrystallites were maintained after SPS. It should be mentioned that the preservation of the nanocrystallites is critical to ensure the enhanced phonon scattering capability even after long-term exposure to the working temperatures in thermoelectric modules. As such, SPS parameters are not a trivial matter. The processing conditions with respect to the temperature and the soaking time are of prime concern and determine the quality of the final product.

3.2. Electrical transport properties

Temperature dependence of the electrical conductivity (σ) and the Seebeck coefficient (S) for $Cu_2CdSnSe_4$ $+x$ vol.% nanocomposites ($x = 0, 1, 3, 5$) are plotted in Fig. 4(a) and (b), respectively. Room-temperature data are listed in Table 1. As shown in Fig. 4(a), the electrical conductivity increases monotonically with the concentration of nanocrystallites, reaching the maximum value of 9240 *S/m* at 439 K when x is 5 vol.%. Compared to the matrix sample, the electrical conductivities of $Cu_2CdSnSe_4$ nanocomposites are enhanced approximately 80%, 89%, and 92% at room temperature for $x = 1$ vol.%, 3 vol.%, and 5 vol.%, respectively. As demonstrated in the above section, $Cu_2CdSnSe_4$ nanocrystallites are present at grain boundaries and surfaces in $Cu_2CdSnSe_4$ nanocomposites. Normally, by introducing nanoinclusions in a bulk material, a drop in the electrical conductivity is expected as each inclusion becomes a scattering center for charge carriers. Surprisingly, in our case, a large improvement in the electrical conductivity occurs, and we will discuss the mechanism for such enhancement in the following section. Meanwhile, it is noted that the electrical conductivities increase with temperature up to 439 K and then decrease for $Cu_2CdSnSe_4$ nanocomposites with $x = 3$ vol.% and 5 vol.%, implying a semiconductor-semimetal transformation at a specific temperature.

Table 1
List of the room-temperature electrical conductivity σ, Seebeck coefficient S, hole concentration p, and mobility μ for $Cu_2CdSnSe_4$ composites ($x = 0$, 1, 3 and 5 vol.%). CS stands for colloidal synthesis method, and the data are cited from Ref. [14].

Sample	S (μVK^{-1})	σ (Sm^{-1})	p (cm^{-3})	μ (cm^2/Vs)
$Cu_2CdSnSe_4$ (matrix)	373	610	2.24×10^{18}	17.02
Matrix+1% nano	190	3102	1.15×10^{19}	16.86
Matrix+3% nano	178	5784	3.61×10^{19}	10.01
Matrix+5% nano	133	7406	4.89×10^{19}	9.47
$Cu_2CdSnSe_4$ (CS)	56	35,321	2.04×10^{20}	10.82

As shown in Fig. 4(b), all samples have a positive Seebeck coefficient, indicating that the majority carriers are holes. The room-temperature Seebeck coefficients of 373, 190, 178 and 133 μV/K were obtained for samples with x equaling 0 vol.%, 1 vol.%, 3 vol.%, and 5 vol.%, respectively. Such differences among the samples are completely consistent with the electrical conductivity behavior. Taking the matrix sample as a reference, the Seebeck coefficients decrease approximately 49%, 52%, and 64% at room temperatures for $x = 1$ vol.%, 3 vol.%, and 5 vol.%, respectively. It is worthwhile to mention that the degree of the S reduction with the increasing x is moderate in contrast to that of the electrical conductivity, allowing for the increase of the power factor (PF) upon the incorporation of $Cu_2CdSnSe_4$ nanocrystallites. The largest value of PF up to 0.31 mWK^{-2} m^{-1} is achieved at 765 K for the sample with $x = 3$ vol.%, which is 53% larger than that of matrix.

It is interesting to note that the room-temperature carrier concentrations of all samples increase with the dispersed $Cu_2CdSnSe_4$ nanocrystallites. As seen in Table 1, the carrier concentration increases from 2.24×10^{18} to 4.89×10^{19} cm^{-3} as x increases from 0 to 5 vol.%, yielding the substantial increase of the electrical conductivity in $Cu_2CdSnSe_4$ nanocomposites compared to that of the matrix. The reason why the carrier concentration is higher in $Cu_2CdSnSe_4$ nanocomposites than in the matrix may be that the $Cu_2CdSnSe_4$ nanocrystallites made via the colloidal synthesis are believed to possess a certain type of deficiency. As a result, a hole

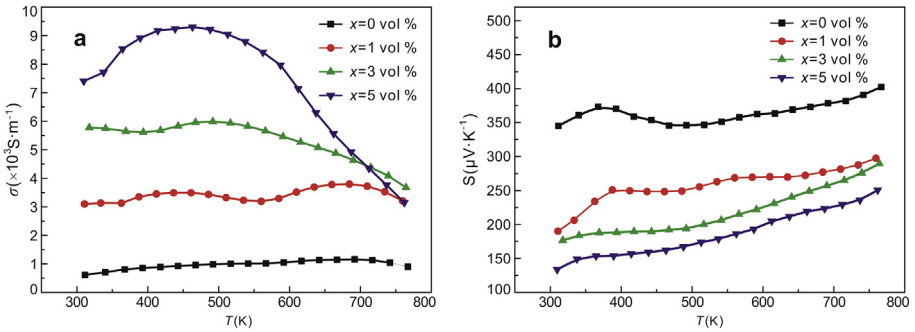

Fig. 4. Temperature dependences of (a) electrical conductivity; (b) Seebeck coefficient for $Cu_2CdSnSe_4$ composites ($x = 0$, 1, 3 and 5 vol.%).

concentration of 2.04×10^{20} cm^{-3} has been obtained, giving a much higher electrical conductivity compared to that of samples by the solid state reaction [14]. The inclusions of such $Cu_2CdSnSe_4$ nanocrystallites may bring more holes to the matrix and lead to the increase of hole concentrations in $Cu_2CdSnSe_4$ nanocomposites.

3.3. Thermal transport properties

Fig. 5 displays the temperature dependence of the thermal conductivity (κ) for samples calculated by $\kappa = \lambda C_p d$. It is noted that the thermal conductivities of all samples decrease with increasing temperature over the measured range up to 773 K. Furthermore, the sample with $x = 1$ vol.% has the lowest thermal conductivity, reaching 0.42 Wm^{-1}K^{-1} at 773 K, which is approximately 35%, 29%, and 33% lower than the matrix, 3% vol.%, and 5 vol.% $Cu_2CdSnSe_4$ composites, respectively. As such, the embedded $Cu_2CdSnSe_4$ nanocrystallites are indeed effective in reducing thermal conductivities of the $Cu_2CdSnSe_4$ matrix due to the enhanced scattering of phonons of mid- to long-wavelengths by the embedded nanocrystallites observed on the grain boundary and surface in $Cu_2CdSnSe_4$ nanocomposites. Furthermore, it is worth noting that the value of κ in the $Cu_2CdSnSe_4$ matrix is lower than that reported by Liu et al. [12], where 1.01 Wm^{-1} K^{-1} was achieved at 700 K. A possible reason for this difference could be the fact that ball milling was applied to our matrix, which results in a powder with reduced particle sizes in the range of 200–500 nm. Thus, a more pronounced grain boundary scattering of phonons in our matrix sample decreases its thermal conductivity with respect to the sample without ball milling as reported by Liu et al.

Thermal conductivity can be divided into two major components: $\kappa = \kappa_e + \kappa_l$, where κ_e is electronic thermal conductivity and κ_l is the lattice part. The electronic thermal conductivity can be described by the Wiedemann-Franz law, $\kappa_e = L\sigma T$, where σ is electrical conductivity, L the Lorenz factor, and T the absolute temperature. Here, we used a single parabolic band to approximate the shape of the valence band in $Cu_2CdSnSe_4$ system [38], and the Lorenz factor, which depends on the degree of elasticity in carrier scattering, can be expressed as [39].

$$L = \left(\frac{k_B}{e}\right)^2 \left[\frac{\left(r+\frac{7}{2}\right)F_{r+\frac{5}{2}}(\xi)}{\left(r+\frac{3}{2}\right)F_{r+\frac{1}{2}}(\xi)} - \left(\frac{\left(r+\frac{5}{2}\right)F_{r+\frac{3}{2}}(\xi)}{\left(r+\frac{3}{2}\right)F_{r+\frac{1}{2}}(\xi)}\right)^2\right] \quad (1)$$

In this equation, e and r are the electron charge and the scattering factor, respectively. r gives the exponent of the energy dependence on the charge carrier mean free path, with a value of $-1/2$ for the acoustic phonon scattering in the $Cu_2CdSnSe_4$ compounds. $F_n(\xi)$ corresponds to the Fermi integral, which can be defined as,

$$F_n(\xi) = \int_0^\infty \frac{x^n}{1+\exp(x-\xi)}\mathrm{d}x \quad (2)$$

where ξ is the reduced Fermi energy that can be deduced from the Seebeck coefficients and the scattering factor based on the following formula,

$$S = \pm\frac{k_B}{e}\left[\frac{\left(r+\frac{5}{2}\right)F_{r+\frac{3}{2}}(\xi)}{\left(r+\frac{3}{2}\right)F_{r+\frac{1}{2}}(\xi)} - \xi\right] \quad (3)$$

In this equation, e is the electron charge. The calculated Lorenz factor as a function of temperature is plotted in the inset of Fig. 5(b). The lattice thermal conductivity is consequently calculated by subtracting the electronic part from the total thermal conductivity, as shown in Fig. 5(b). It is noted that due to the relatively low electrical conductivity in $Cu_2CdSnSe_4$ compounds, κ_e takes a very small fraction in the total thermal conductivity. In addition, lattice thermal conductivities follow approximately the $1/T$ relation [dashed line in Fig. 5(b)], and all samples exhibit noticeably low values. As noted in the introduction section, these low lattice thermal conductivities in $Cu_2CdSnSe_4$-based compounds can be ascribed to: (1) the complex chemical-bonding and the highly distorted diamond-like structure and (2) grain size reduction via the ball milling process leading to the enhanced grain boundary scattering and reduced lattice thermal conductivities. Additionally, the lattice thermal conductivities display a similar trend for the total conductivities: a dramatic reduction in lattice thermal conductivities is obtained by introducing

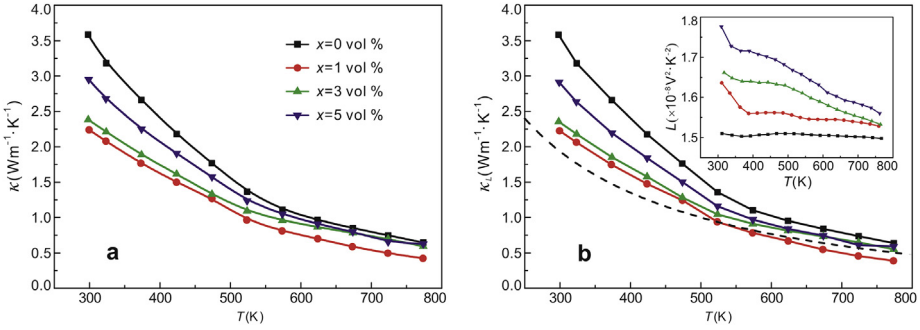

Fig. 5. Temperature dependences of (a) thermal conductivities, (b) lattice thermal conductivities for $Cu_2CdSnSe_4$ nanocomposites ($x = 0$, 1, 3 and 5 vol.%). The dashed line is the theoretical 1/T relation, and the inset of (b) is the calculated temperature-dependent of the Lorenz number L.

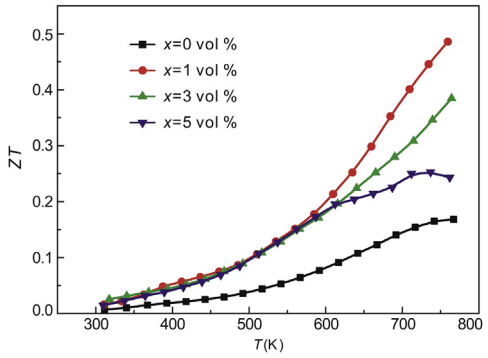

Fig. 6. *ZT* as a function of temperature for $Cu_2CdSnSe_4$ composites ($x = 0$, 1, 3 and 5 vol.%).

homogeneous nanoinclusions into the $Cu_2CdSnSe_4$ matrix. By taking $x = 1$ vol.% as a reference, the lattice thermal conductivity is reduced approximately 41% at 773 K in comparison to that of the matrix sample. It is believed that these homogeneous nanoinclusions act as extra scattering centers, which can largely scatter phonons with both mid- and long-wavelengths. Obviously, the reduction in the lattice thermal conductivity upon the presence of $Cu_2CdSnSe_4$ nanocrystallites far exceeds the concomitant increase in the electronic thermal conductivity and results in the overall reduction in the total thermal conductivity for $Cu_2CdSnSe_4$ nanocomposites.

The dimensionless thermoelectric figure of merit *ZT* is calculated based on the above transport data and plotted in Fig. 6. It is found that the *ZT* values increase with increasing temperature in the entire measured temperature range. Furthermore, the presence of homogeneous $Cu_2CdSnSe_4$ nanoinclusions in the matrix leads to the simultaneous optimization in both the power factor and the thermal conductivity, resulting in a remarkable increase in *ZT* with a maximum of ~0.5 at ~760 K for the sample with $x = 1$ vol.%, approximately triple that of the $Cu_2CdSnSe_4$ matrix. The enhancement of the figure of merit for the $Cu_2CdSnSe_4$ composites can be ascribed to: (1) $Cu_2CdSnSe_4$ nanoinclusions, distributed on grain surfaces and boundaries, donate more holes into the matrix and boost the carrier density as well as the electrical conductivity; and (2) the ex-situ homogeneous $Cu_2CdSnSe_4$ nanocrystallites associated with the reduced grain size increase phonon scattering, resulting in a lower thermal conductivity.

4. Conclusion

$Cu_2CdSnSe_4$ composites containing homogeneous $Cu_2CdSnSe_4$ nanocrystallites have been synthesized by ball milling and subsequent spark plasma sintering. They show very good thermoelectric performance with the highest *ZT* value reaching 0.5 at 760 K when dispersing 1 vol.% $Cu_2CdSnSe_4$ nanocrystallites, which have uniform particle sizes with diameters ranging from 20 to 30 nm as prepared. The observed enhancement in the electrical conductivity along with a significant reduction in the lattice thermal conductivity leads to an improved *ZT* in $Cu_2CdSnSe_4$ composites. This strategy to synthesize nanocomposites with ex-situ homogeneous nanoinclusions shows great potential in enhancing the thermoelectric performance of both quaternary chalcogenide $Cu_2CdSnSe_4$ and other desirable TE materials.

Acknowledgments

This work was financially supported in part by the National Natural Science Foundation of China (Grant no. 51472036, 51401202, 11404044). Work at the Chongqing Institute of Green and Intelligent Technology, Chinese Academy of Sciences was supported by the One Hundred Person Project of the Chinese Academy of Science, Grant No. 2013-46. YC and JYD are grateful for the financial support of the Hong Kong Polytechnic Strategic Importance Scheme (Grant no.1-ZVCG).

References

[1] Uher C. Semiconductors and semimetals. In: Recent trends in thermoelectric materials research; 2001. p. 139–253.
[2] Caillat T, Borshchevsky A, Fleurial JP. Properties of single crystalline semiconducting $CoSb_3$. J Appl Phys 1996;80:4442–9.
[3] Chen BX, Xu J-H, Uher C, Morelli DT, Meisner GP, Fleurial J-P, et al. Low-temperature transport properties of the filled skutterudites $CeFe_{4-x}Co_xSb_{12}$. Phys Rev B 1997;55:1476–80.
[4] Chen LD, Kawahara T, Tang XF, Goto T, Hirai T, Dyck JS, et al. Anomalous barium filling fraction and n-type thermoelectric performance of $Ba_yCo_4Sb_{12}$. J Appl Phys 2001;90:1864–8.
[5] Li H, Tang XF, Zhang QJ, Uher C. High performance $In_xCe_yCo_4Sb_{12}$ thermoelectric materials with in situ forming nanostructured InSb phase. Appl Phys Lett 2009;94:102114.
[6] Zhao L-D, Tan GJ, Hao SQ, He JQ, Pei YL, Chi H, et al. Ultrahigh power factor and thermoelectric performance in hole-doped single-crystal SnSe. Science 2016;351:141–4.
[7] Morelli DT, Meisner GP. Low temperature properties of the filled skutterudite $CeFe_4Sb_{12}$. J Appl Phys 1995;77:3777–81.
[8] Pei YZ, Shi XY, LaLonde A, Wang H, Chen LD, Snyder GJ. Convergence of electronic bands for high performance bulk thermoelectrics. Nature 2011;473:66–9.
[9] Zou TH, Qin XY, Li D, Li LL, Sun GL, Wang QQ, et al. Enhanced thermoelectric performance of β-Zn_4Sb_3 based composites incorporated with large proportion of nanophase Cu_3SbSe_4. J Alloy Compd 2014;588:568–72.
[10] Zhang X, Zhao LD. Thermoelectric materials: energy conversion between heat and electricity. J Materiomics 2015;1:92–105.
[11] Zhao L-D, Hao SQ, Lo S-H, Wu C-I, Zhou XY, Lee Y, et al. High thermoelectric performance via hierarchical compositionally alloyed nanostructures. J Am Chem Soc 2013;135:7364–70.
[12] Liu M-L, Chen I-W, Huang F-Q, Chen L-D. Improved thermoelectric properties of cu-doped quaternary chalcogenides of $Cu_2CdSnSe_4$. Adv Mater 2009;21:3808–12.
[13] Fan F-J, Yu B, Wang Y-X, Zhu Y-L, Liu X-J, Yu S-H, et al. Colloidal synthesis of $Cu_2CdSnSe_4$ nanocrystals and hot-pressing to enhance the thermoelectric figure-of-merit. J Am Chem Soc 2011;133:15910–3.
[14] Chen QF, Wang GW, Zhang AJ, Yang DF, Yao W, Peng KL, et al. Colloidal synthesis of $Cu_{2-x}Ag_xCdSnSe_4$ nanocrystals: microstructures facilitate high performance thermoelectricity. J Mater Chem C 2015;3:12273–80.
[15] Zhou XY, Wang GY, Zhang L, Chi H, Su XL, Sakamoto J, et al. Enhanced thermoelectric properties of Ba-filled skutterudites by grain size reduction and Ag nanoparticle inclusion. J Mater Chem 2012;22:2958–64.

[16] Zhou XY, Wang GW, Guo LJ, Chi H, Wang GY, Zhang QF, et al. Hierarchically structured TiO_2 for Ba-filled skutterudite with enhanced thermoelectric performance. J Mater Chem A 2014;2:20629–35.
[17] Cederkrantz D, Farahi N, Borup KA, Iversen BB, Nygren M, Palmqvist AEC. Enhanced thermoelectric properties of Mg_2Si by addition of TiO_2 nanoparticles. J Appl Phys 2012;111:023701.
[18] Brochin F, Lenoir B, Devaux X, Martin-Lopez R, Scherrer H. Preparation and transport properties of polycrystalline Bi and Bi-SiO_2 nanocomposites. J Appl Phys 2000;88:3269–75.
[19] Huang XY, Xu Z, Chen LD. The thermoelectric performance of ZrNiSn/ZrO_2 composites. Solid State Commun 2004;130:181–5.
[20] Katsuyama S, Watanabe M, Kuroki M, Maehata T, Ito M. Effect of NiSb on the thermoelectric properties of skutterudite $CoSb_3$. J Appl Phys 2003;93:2758–64.
[21] Li Z-Y, Li J-F, Zhao W-Y, Tan Q, Wei T-R, Wu C-F, et al. PbTe-based thermoelectric nanocomposites with reduced thermal conductivity by SiC nanodispersion. Appl Phys Lett 2014;104:113905.
[22] Zou TH, Qin XY, Li D, Sun GL, Dou YC, Wang QQ, et al. Simultaneous enhancement in thermoelectric power factor and phonon blocking in hierarchical nanostructured β-Zn_4Sb_3-Cu_3SbSe_4. Appl Phys Lett 2014;104:013904.
[23] Snyder GJ, Toberer ES. Complex thermoelectric materials. Nat Mater 2008;7:105–14.
[24] Dresselhaus MS, Chen G, Tang MY, Yang RG, Lee H, Wang DZ, et al. New directions for low-dimensional thermoelectric materials. Adv Mater 2007;19:1043–53.
[25] Bux SK, Fleurial J-P, Kaner RB. Nanostructured materials for thermoelectric applications. Chem Commun 2010;46:8311–24.
[26] Vineis CJ, Shakouri A, Majumdar A, Kanatzidis MG. Nanostructured thermoelectrics: big efficiency gains from small features. Adv Mater 2010;22:3970–80.
[27] Yu B, Zhang QY, Wang H, Wang XW, Wang HZ, Wang DZ, et al. Thermoelectric property studies on thallium-doped lead telluride prepared by ball milling and hot pressing. J Appl Phys 2010;108:016104.
[28] Volobujeva O, Raudoja J, Mellikov E, Grossberg M, Bereznev S, Traksmaa R. Cu2ZnSnSe4 films by selenization of Sn–Zn–Cu sequential films. J Phys Chem Solids 2009;70:567–70.
[29] Altosaar M, Raudoja J, Timmo K, Danilson M, Grossberg M, Krustok J, et al. Cu2Zn1-xCdxSn(Se1-ySy)4solid solutions as absorber materials for solar cells. Phys Stat Sol (a) 2008;205:167–70.
[30] Yang CC, Li S. Size-dependent Raman red shifts of semiconductor nanocrystals. J Phys Chem B 2008;112:14193–7.
[31] Zeiri L, Patla I, Acharya S, Golan Y, Efrima S. Raman spectroscopy of ultranarrow CdS nanostructures. J Phys Chem C 2007;111:11843–8.
[32] Kanatzidis MG. Nanostructured thermoelectrics: the new paradigm? Chem Mater 2009;22:648–59.
[33] Lan YC, Minnich AJ, Chen G, Ren ZF. Enhancement of thermoelectric figure-of-merit by a bulk nanostructuring approach. Adv Funct Mater 2010;20:357–76.
[34] Xie WJ, He J, Kang HJ, Tang XF, Zhu S, Laver M, et al. Identifying the specific nanostructures responsible for the high thermoelectric performance of (Bi, Sb)$_2Te_3$ nanocomposites. Nano Lett 2010;10:3283–9.
[35] Vaqueiro P, Powell AV. Recent developments in nanostructured materials for high-performance thermoelectrics. J Mater Chem 2010;20:9577–84.
[36] Minnich AJ, Dresselhaus MS, Ren ZF, Chen G. Bulk nanostructured thermoelectric materials: current research and future prospects. Energy Environ Sci 2009;2:466–79.
[37] Zhao L-D, Dravid VP, Kanatzidis MG. The panoscopic approach to high performance thermoelectrics. Energy Environ Sci 2014;7:251–68.
[38] Zhang JW, Liu RH, Cheng N, Zhang YB, Yang JH, Uher C, et al. High-performance pseudocubic thermoelectric materials from non-cubic chalcopyrite compounds. Adv Mater 2014;26:3848–53.
[39] Dahal T, Jie Q, Lan YC, Guo CF, Ren ZF. Thermoelectric performance of Ni compensated cerium and neodymium double filled p-type skutterudites. Phys Chem Chem Phys 2014;16:18170–5.

Miss Qiufan Chen, Chongqing University, Email: qfchen1991@foxmail.com. Qiufan Chen is a master student at Chongqing University, China. Her research is focused on developing and synthesizing thermoelectric materials and measuring their properties, especially in quaternary chalcogenides. She received a B. Sc. from Xinyang Normal University, China and a M. S. from Chongqing University, China.

Professor Xiaoyuan Zhou, Chongqing University, Email: xiaoyuan2013@cqu.edu.cn. Xiaoyuan Zhou is a professor at Chongqing University, China. Her research interests cover advanced thermoelectric materials, lithium battery and other energy devices. She obtained her Ph.D. degree from The Hong Kong Polytechnic University, in 2008. After obtaining her Ph.D., she worked as a postdoctoral fellow at University of Washington (2008–2010) and University of Michigan (2010–2013), USA. She has so far published about 50 papers, and over 500 citations are received.

Associate Professor Xiaonan Sun, Chongqing University, Email: xnsun168@cqu.edu.cn. Xiaonan Sun is an associate professor at Chongqing University, China. His recent research focuses on environmental physics and its applications. He received a B. E. and a Ph. D both from Chongqing University, China. He now works as a director of the institute of environmental physics, Chongqing University.